



HAL
open science

Permittivity measurement of cementitious materials with an open-ended coaxial probe

Vincent Guihard, Frédéric Taillade, Jean-Paul Balayssac, Barthélémy Steck,
Julien Sanahuja, Fabrice Deby

► **To cite this version:**

Vincent Guihard, Frédéric Taillade, Jean-Paul Balayssac, Barthélémy Steck, Julien Sanahuja, et al..
Permittivity measurement of cementitious materials with an open-ended coaxial probe. *Construction
and Building Materials*, 2020, 230, pp.116946. 10.1016/j.conbuildmat.2019.116946 . hal-02462363

HAL Id: hal-02462363

<https://hal.insa-toulouse.fr/hal-02462363>

Submitted on 20 Jul 2022

HAL is a multi-disciplinary open access archive for the deposit and dissemination of scientific research documents, whether they are published or not. The documents may come from teaching and research institutions in France or abroad, or from public or private research centers.

L'archive ouverte pluridisciplinaire **HAL**, est destinée au dépôt et à la diffusion de documents scientifiques de niveau recherche, publiés ou non, émanant des établissements d'enseignement et de recherche français ou étrangers, des laboratoires publics ou privés.



Distributed under a Creative Commons Attribution - NonCommercial 4.0 International License

Permittivity measurement of cementitious materials with an open-ended coaxial probe

Vincent Guihard^{1,2}, Frédéric Taillade¹, Jean-Paul Balayssac², Barthélémy Steck¹, Julien Sanahuja¹, and Fabrice Deby²

¹EDF R&D, 6 quai Watier, 78401 Chatou Cedex, France

²LMDC, INSA/UPS Génie Civil, 135 Avenue de Rangueil, 31077 Toulouse cedex 04 France

Abstract

This study presents a methodology to investigate the complex permittivity of heterogeneous samples like concrete, mortars and cement pastes by using an open-ended coaxial probe. The probe is associated with portable Vector Network Analyser (VNA) allowing in-situ measurements. Another advantage of the proposed methodology is that the complex permittivity of concrete can be assessed from the measurement of the reflection parameter S_{11} alone which is innovating in comparison with common devices. This can be achieved by modelling the electrical equivalent circuit of the coaxial probe and the dielectric sample with a capacitive model briefly presented in this paper. A calibration procedure on materials with known permittivity developed to estimate the input parameters of the capacitive model is presented in this paper meanwhile all the details of measurements. Measurements performed on various cementitious materials (cement paste, mortar and concrete) at different degrees of water saturation (from almost dry to fully saturated) show that the probe is able to characterize their dispersive behavior. It is also demonstrated that the probe is able to measure both real and imaginary permittivity of cementitious materials in an extended range of moisture. Relationships are proposed between real or imaginary permittivity and volume water content.

Keywords

Permittivity, coaxial probe, dispersive behavior, cement paste, mortar, concrete, porosity, moisture

1. Introduction

Water content of cementitious materials is one of the most important parameters to describe their durability. Water content of cementitious materials can be deduced from permittivity measurement at different frequencies from 30 MHz up to 2 GHz [1]. The present study is part of a project aiming to predict the water content of aging as well as new concrete buildings, thanks to permittivity measurements made on the bulk material and its constituents. Among all electromagnetic devices available to assess the permittivity of dispersive dielectrics, coaxial line transmission and reflection based instruments are among the most commonly used. Dielectric permittivity can be derived from

the analysis of transmission or reflection of electromagnetic waves through a sample inserted into a coaxial structure [2]. Coaxial transmission lines have been extensively studied and present numerous benefits, e.g. broad frequency range and capability to measure both reflection and transmission coefficients of a sample. These coefficients enable both the dielectric constant and the magnetic susceptibility to be measured. However, they only allow ex-situ measurement, requiring extraction of samples from the original bulk material. This method is hence not suitable for some applications, including the non-destructive evaluation of civil engineering structures. Methods based on wave reflection do not necessarily require any sample collection. These reflection phenomena are induced by an impedance discontinuity, which, in turn, is caused by the sample located at the end of a coaxial line.

Open-ended coaxial probes are one of the methods reviewed, along with many others, in [2] and [3]. They are simple to implement and have a broad frequency range driven by the network analyzer used to synthesize the RF signal. However, since transmission coefficients are necessary to determine both the magnetic and dielectric properties of materials, reflection probes are essentially reserved for permittivity measurement of non-magnetic materials. The non-destructive and non-invasive characteristics of such tools have enabled investigations of different kinds of media, such as biological tissues and liquids [4] [4] [3] [6] [7], agricultural products [8] [9], soils [10] [11] [12], and also flat surfaces of solid samples like concrete [13] [14] or, more recently, artificially grown sea ice [15]. The probes exist in different configurations and can be chosen according to the sample position within the system. They are summarized in [3] and [16] and have all been studied over recent decades to fully understand wave propagation mechanisms and calculate dielectric properties of materials from the measured signal reflection. Among the different studies dedicated to such systems, numerical simulations of probe operation have been extensively performed using both Finite Element Method (FEM) or Method Of Moment (MOM) calculation processes [8] [17] [18] [19] [20] [21] [22].

The approach developed in this study shows that a simple capacitive model describing the behavior of the probe enables the permittivity of flat samples to be calculated. We present a conical probe designed to investigate heterogeneous materials and a new two-dimensional axisymmetric FEM model developed to validate this approach over specific frequency ranges. Measurements were performed on various cementitious materials (cement paste, mortar and concrete) and the results for the real and imaginary parts of the permittivity are presented.

2. Design of the large, open-ended coaxial probe

The use of a coaxial probe to deduce the permittivity of a dielectric material from the amount of energy reflected on its surface calls upon transmission line theory [2]. This concept enables an accurate

description of electromagnetic wave propagation through a coaxial cable and is the basis for understanding how the probe operates.

A typical coaxial cable is composed of two concentric cylindrical structures made of a conducting material (a center core and a metallic shield) separated by a dielectric insulator. Parameters a and b will be used in the following to represent the radii of the metallic core and shield, respectively. In such cables, transverse electromagnetic (TEM) modes are the only propagation modes allowed within the dielectric material. Thus, both the electric and magnetic components of an incident wave are exclusively located in the plane perpendicular to the propagation direction. The same basic structure is used to build open-ended coaxial probes.

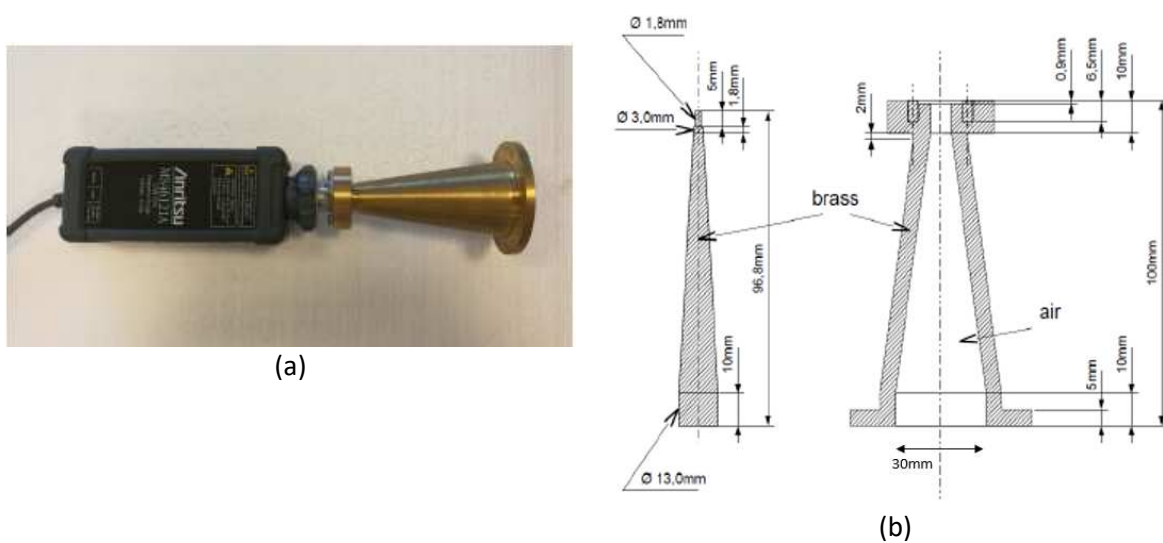


Figure 1: Open-ended coaxial probe

Figure 1a shows a photograph of the probe designed and the Anritsu MS46121 vector network analyzer used during the study. The probe is characterized by a metallic core of radius $a = 6.5$ mm and dielectric insulator of radius $b = 15$ mm at the end of the probe. The large diameter of the dielectric (30 mm) enables the investigated volume to be expanded in order to perform measurements on heterogeneous samples characterized by large representative elementary volumes (REV). These volumes are defined according to the largest heterogeneity size contained within the material under test. Also, because of the conical shape of the device, values a and b vary along the probe length but the ratio b/a remains constant, thus maintaining the probe characteristic impedance, Z_0 , equal to 50Ω and preventing any reflection within the probe.

Figure 1b presents a cross sectional view of the device. The brass core and shield are kept together at the top of the probe by an N connector filled with Teflon and also having a 50Ω characteristic impedance. The device is directly connected to the vector network analyzer (VNA). The only reflection

detected has to come from the sample placed below the probe. If the impedance of the material is not equal to 50Ω , the system composed of the probe and sample is equivalent to a lossless transmission line terminated by a load impedance Z_L , which depends on the electromagnetic properties of the sample. This approximation is restricted to the case of a semi-infinite sample i.e. a sample deep enough to ensure that the amplitude of the electric field E is at least two orders of magnitude lower at the end of the sample than at the interface with the probe [3]. Komarov et al. [15] recall that wave propagation through the sample can be seen as a distortion of the TEM signal in the vicinity of the probe aperture. This would induce the appearance of a component of the electric field perpendicular to the aperture and a radiation of the wave into the sample. Partial reflection of the energy towards the probe is then observed. Eq.1 can be used to link the S_{11} parameter, measured with the VNA, and the impedance of a sample, such that

$$S_{11} = \frac{Z_L - Z_0}{Z_L + Z_0} \quad (\text{Eq. 1})$$

with, Z_L : Load impedance

$Z_0=50 \Omega$, characteristic impedance of the probe

This reflection coefficient is known to be a function of the electromagnetic properties of the sample under test [13], [22], [23], [24]. Many models have been developed during recent decades to determine the dielectric constant or the magnetic permeability of semi-infinite materials by measuring a voltage reflection coefficient. For simple system geometry, dielectric permittivity can sometimes be derived from the integral expression of the admittance at the end of the coaxial probe [25]. However, it is acknowledged [13] that the vast computing resources needed in such cases makes instant measurements impossible. To simplify the expression of impedance at the end of the probe, other approaches have been used: the quasi-static approach, the Taylor-series development approach, or equivalent electrical circuit approaches. The latter assume that the measurement circuit is similar to a classic electrical circuit. Chen et al., [2] review the most famous of these models: the capacitive model [3], the antenna model [26], the virtual line model [27] and the rational function model. Such models offer immediate permittivity calculation but also present drawbacks such as limited frequency range suitability.

3. Measurement and result processing

3.1. Measurement procedure

The vector network analyzer used in this study was an Anritsu MS46121 with a signal frequency range set to [1 MHz; 2 GHz]. Measurement of the S_{11} parameter over this broad range was performed on materials with known permittivity, such as air and Teflon, and also on materials with unknown

electromagnetic properties, such as rock aggregate, cement paste, mortar, and concrete, as presented in Figure 2. A VNA calibration procedure was required before the probe was set up, in order to take external factors influencing the device operation into account, e.g. temperature or hygrometry. This was performed by measuring the reflected signal on three different loads (open circuit, short circuit and 50Ω load impedance). It is also necessary to recall that the default configuration of the reference plane of the VNA after calibration is defined at the output of the device. S_{11} parameters should be measured at this exact position. In the present study, this reflection coefficient had to be measured at the interface between the probe and the sample because the phase deployed itself over the additional line length induced by the probe. So a change of reference plane was performed by plugging the probe in and short-circuiting it by placing a conductive material (a copper foil in this case) at its end.



Figure 2. Acquisition of the S_{11} parameter on the surface of a concrete sample.

3.2. Capacitive model

Estimating the dielectric permittivity of the material under test from the impedance value Z_L then required the use of a specific model. Here, the capacitive model [3] presented in Figure 3 was used.

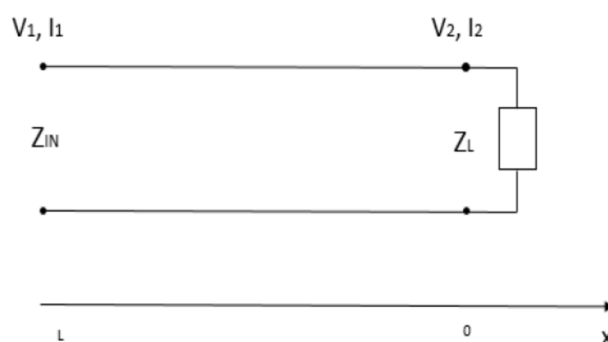


Figure 3: Electrical equivalent circuit of a coaxial probe and dielectric sample according to the capacitive model

This circuit comprises two capacitors C_f and $C(\varepsilon_r^*) = \varepsilon_r^* \cdot \chi$ connected in parallel. Capacitor $C(\varepsilon_r^*)$ is used to model the electric energy storage capacity of the sample. The complex value of the permittivity ε_r^* allows the dielectric losses within the material to be taken into consideration. The χ factor is a geometric factor used to take account of the geometry of the probe. The capacitor C_f is often used to interpret the energy storage capacity due to the fringing fields. This capacity is material independent and comes only from the fact that fringing fields exist at the boundaries of every non-infinite planar capacitor [28]. Parameters χ and C_f being difficult to estimate, a calibration procedure using well-known materials is necessary. Using Eq. 1, an expression describing the permittivity of a sample placed at the end of the coaxial probe can be deduced,

$$\varepsilon_r^* = \frac{1-S_{11}}{j\omega Z_0 \chi (1+S_{11})} - \frac{C_f}{\chi} \quad (\text{Eq.2})$$

It is possible to eliminate the two unknown parameters χ and C_f by measuring the S_{11} parameter on two materials of known permittivity (ε_1^{ref} and ε_2^{ref}). The resulting expression for the dielectric constant of an unknown sample is then given by,

$$\varepsilon_r^* = \varepsilon_{r1}^{ref} + (\varepsilon_2^{ref} - \varepsilon_1^{ref}) \left(\frac{Y_r - Y_1^{ref}}{Y_2^{ref} - Y_1^{ref}} \right) \quad (\text{Eq.3})$$

The two reference materials used in this study were air ($\varepsilon_{air} = 1 + 0j$) and a 25x15x10 cm Teflon block ($\varepsilon_{teflon} = 2.1 + 0j$).

The use of the capacitive model had been validated in a previous study by using a numerical model and measurements on rock samples [29]. The material, of dimensions 14x7x9 cm, was a homogeneous block of aggregate commonly used as one of the components of concrete. The frequency range chosen was [1 MHz; 2 GHz]. The permittivity deduced from the measurement of the S parameters on the flat surface of the block is presented in Figure 4. The real part lies between 4 and 5 at low frequencies and increases slightly at high frequencies. The imaginary part is almost equal to 0 at low frequencies and also seems to increase at high frequencies. It was observed that the permittivity deviation was probably caused by the measuring system and the capacitive model, and increased with the difference between the permittivity value of the material under test and the permittivity of the dielectric filling the probe (air in this case) [30].

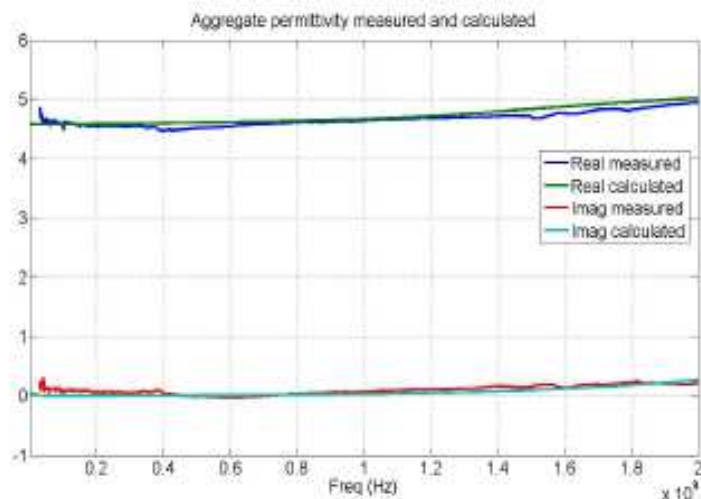


Figure 4: Measurement of the real and imaginary parts of the permittivity of a rock sample.

3.3 Effective penetration depth

Many experiments have been performed in order to estimate the effective penetration depth of waves in a sample [32] [21] [33] [34]. This effective penetration depth is closely related to the probe diameter [32] and is in the same order of magnitude as this diameter [21]. Meany et al., [32] computed the evolution of the penetration depth as a function of probe diameter, frequency and medium permittivity. The probe diameter was found to be the most influential parameter and penetration depth was almost constant with frequency and sample permittivity [32]. The effective penetration depth is an important characteristic especially when dealing with heterogeneous samples like concrete. The Representative Elementary Volume (REV) is usually defined as the minimum dimensions of the volume investigated by the probe so that the measurement can be considered representative. This volume is closely related to the maximum size of the heterogeneities contained in the studied material (around three times the volume of these heterogeneities). Hence, care must be taken when studying materials with quite large heterogeneities like concrete. A probe with a larger diameter might be necessary to study concrete samples comprising aggregates a few centimeters in size. Figure 5 presents the real part of the permittivity resulting from a simulation performed with a heterogeneous sample made of two layers having different permittivities in the aim of estimating the wave penetration depth. The upper layer was made of a material with permittivity $5 + 0j$. The lower material was air ($\epsilon = 1 + 0j$). We computed the effective permittivity following the described procedure for various sample thicknesses, e . Results showed that, for samples with permittivity $5 + 0j$ that were thinner than 2 cm, the resulting permittivity was different from $5 + 0j$. Effective penetration depth hence lay around 2cm. In the following, the maximum diameter of aggregates for concrete mixes is

equal to 11 mm which is the same range as the depth penetration of the probe, but less than the REV, which should be at least three times the maximum size of the aggregates. To quantify the variability, at least six measurements are performed and averaged to provide a value of permittivity. The coefficient of variation obtained is always less than 11%.

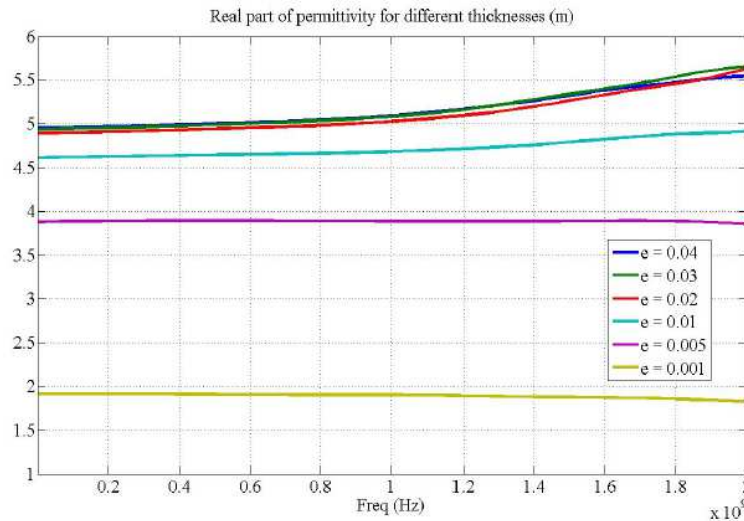


Figure 5: Assessment of the effective penetration depth

4. Experimental details

4.1. Materials

Tables 1, 2 and 3 present the details of the mixes used in this study. Different cement pastes were tested with different water to cement ratios in order to obtain a significant range of porosity. Different mixes of mortar were designed by using a 0/2 mm sand and changing the sand to cement ratio in order to modify the volume of paste and aggregates. For mortars M1 and M2, the proportion of cement paste was 51% for mortar Mm1 and 43% for Mm2. A concrete with a water to cement ratio of 0.62 and a superplasticizer were also characterized.

Table 1: Cement paste properties

Mix	CP 0.28-1	CP 0.28-2	CP 0.34-1	CP 0.34-2	CP 0.4-1	CP 0.4-2
W/C	0.28	0.28	0.34	0.34	0.40	0.40
Porosity (%)	26.7	26.5	31.7	31.8	35.9	36.0

Table 2: Mortar properties

Mix	M1	M2	Mm1	Mm2
S/C	2.1		3	
Cement (kg/m ³)	595		500	
W/C	0.53		0.53	
Porosity (%)	22.4	22.4	18.6	19.6

Table 3: Concrete (C) properties

Cement (kg/m ³)	315
Sand 0-4 (kg/m ³)	819
Fine Gravel 4-11 (kg/m ³)	978
Water (kg/m ³)	194
Superplasticizer (kg/m ³)	2.6
W/C	0.62
Density (kg/m ³)	2320
Slump (cm)	15.5
Porosity (%)	13.9

The cement used was a CEM I 52.5 N from a factory (Italcementi) at Gaurin in France. Alluvial sand-lime aggregates were used, a 0/4 mm sand (for mortar and concrete) and a fine, 4/11 mm, gravel (for concrete). The superplasticizer used for concrete was Sikaplast Techno 80 from SIKA.

The porosity was measured by applying the procedure defined in [31]. The range of porosity was between 26.5 and 36.0% for cement pastes and between 18.6 and 22.4% for mortars. The porosity of the concrete was 13.9%, so, globally, the mixes covered a range of porosity from 14% to 36%. All the mixes were cured under water for 28 days.

For cement pastes and mortars, two cubes (8 cm*8cm*8cm) per mix were cast. For concrete three cylinders (diameter 11.5 cm and height 23 cm) were cast. After 28 days of curing, the cylinders were cut into 3 slices (6 cm thick). The permittivity measurements were realized on the three slices and averaged for each sample.

To change the saturation degree of the samples, a conditioning procedure was applied. From the full-saturation state, the samples under test were progressively dried at 60 °C to reach the following saturation degrees:

- 90%, 80%, 70%, 60%, 50%, 40%, 30% for cement pastes,
- 90%, 80%, 60%, 50%, 40%, 30%, 20% for mortars,
- 90%, 80%, 70%, 60%, 36% for concrete.

Once the mass corresponding to the saturation degree was reached, the sample was sealed in adhesive aluminum foil and kept at 60 °C for the duration of drying. This process enabled the water content inside the sample to become homogeneous. Then, the sample was tested with the coaxial probe and the procedure was repeated for the next saturation degree.

4.2. Measurements

For each saturation degree, permittivity measurements were performed on the six faces of each sample with the open-ended coaxial probe. Good contact being required between the probe and the sample to avoid measurement bias [29], the probe has to be held tightly on the surface of the material by the operator. The data acquired on all faces was then averaged and could be displayed as a function of frequency. Low standard deviation was observed when six measurements were performed at different positions on a rock sample. As an example, the mean value of the real and the imaginary parts of the permittivity acquired on this rock sample is presented Figure 6 and shows the good reproducibility of the measurement procedure.

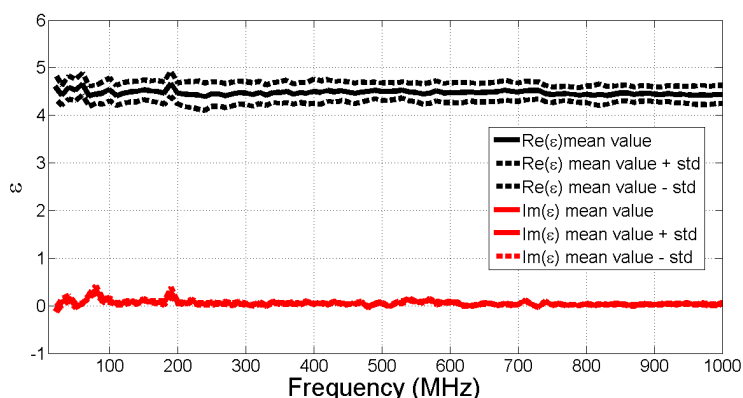


**Figure 6: Measurement results obtained at six positions on a rock sample
(mean and standard deviation)**

5. Results and discussion

5.1. Cement pastes

Figure 7 presents the variation of the real and imaginary parts of the permittivity (mean of the measurements performed on the six faces of the two samples) versus the frequency for saturation degrees of 100% and 30%.

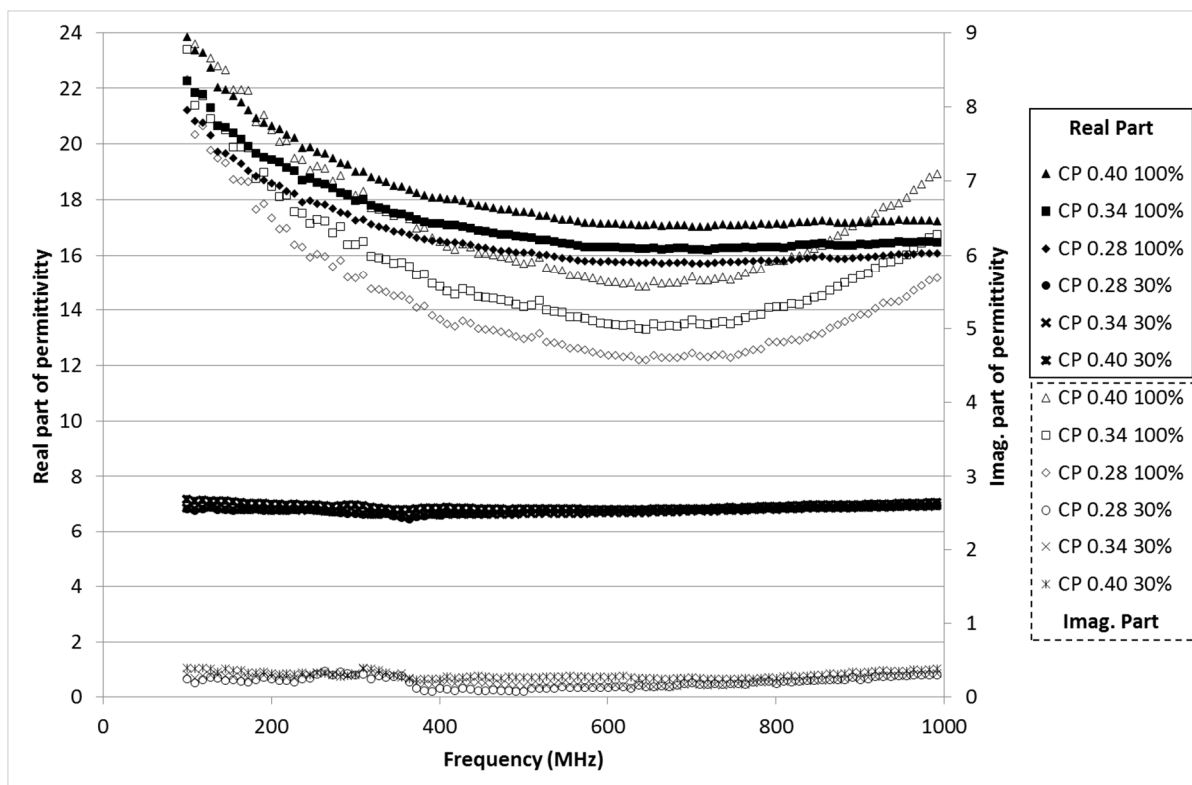


Figure 7: Real and imaginary parts of the permittivity measured on cement pastes for saturation degrees of 100% and 30%

It can be observed that the variation of the permittivity (real and imaginary) versus the frequency is linked to moisture. The permittivity is frequency-dependent for high moisture content while it does not depend on frequency when the porosity is weakly saturated. This confirms the results already obtained on concrete by Dérobert et al. [30]. Moreover it can be observed that the real part of the permittivity is almost independent of frequency in the range of [500-1000 MHz] even if the material is fully saturated. On the other hand, the imaginary part increases between 500 and 1000 MHz, especially when the cement pastes are fully saturated. This was already observed on a rock sample and could be attributed to a limit of the capacitive model of the probe [29]. The measurement is also sensitive to the water to cement ratio for 100% saturation. It can be observed in Table 1 that the porosity increases with the water to cement ratio. When the mix is fully saturated, the quantity of water is equal to the porosity, so it increases with the water to cement ratio. It can be noted that both the real and imaginary

parts of permittivity increase with the quantity of moisture, which is also in agreement with previous results [30], [35], [36]. This effect is not so sensitive for a saturation degree of 30% because the quantity of water inside the porosity is not great enough. The same comparison can be made between the two saturation degrees of a given water to cement ratio. For instance, at 1000 MHz, the real part of the permittivity of mix CP 0.28 changes from 16 to 6.5 for saturation degrees of 100 and 30% respectively. For the imaginary part, these values are 5.7 and 2.6 respectively.

Figure 8 presents the variation of the real and imaginary parts of the permittivity versus the saturation degree. In this case it was decided to calculate the mean of all the measured values in the range of [500 – 1000 MHz] instead of considering only a value for one frequency. Moreover, this frequency range corresponds to the usual GPR frequencies used for the characterization of concrete. The error bars represent the standard deviation calculated from twelve measurements (one per face of the two available cubes). It is clear that the permittivity (real and imaginary) decreases with the saturation degree. It seems, however that the relationship between the two is not proportional throughout the range of saturation. Although the relationship is fairly linear between 30% and 80%, which is in agreement with the literature [30], [35], there is a more marked increase of permittivity between 80% and 100%. This could be due to the effect of macro porosity, which is only filled for the higher moisture content and which could induce a higher increase of the volume water content. An additional measurement at a saturation degree of 95% could confirm this assumption.

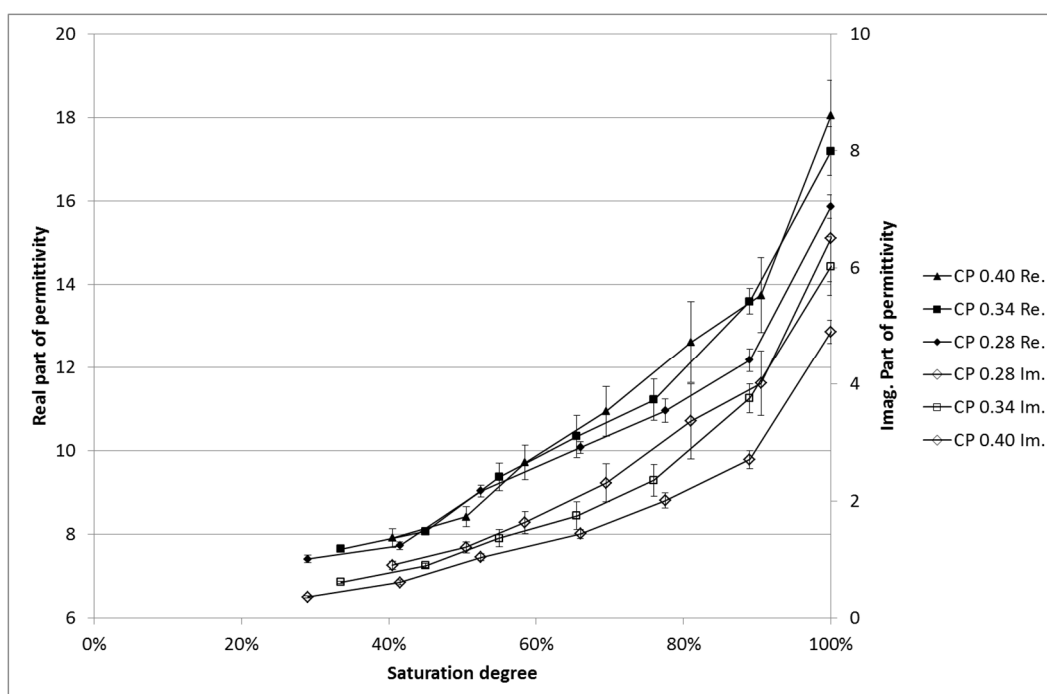


Figure 8: Variation of real and imaginary part of permittivity (mean in the range 500-1000 MHz) versus saturation degree (all the cement pastes)

5.2. Mortars

Figure 9 gives the variation of permittivity versus frequency for mortars (mean of values measured on the six faces of the two samples) at two saturation degrees (100 and 30%).

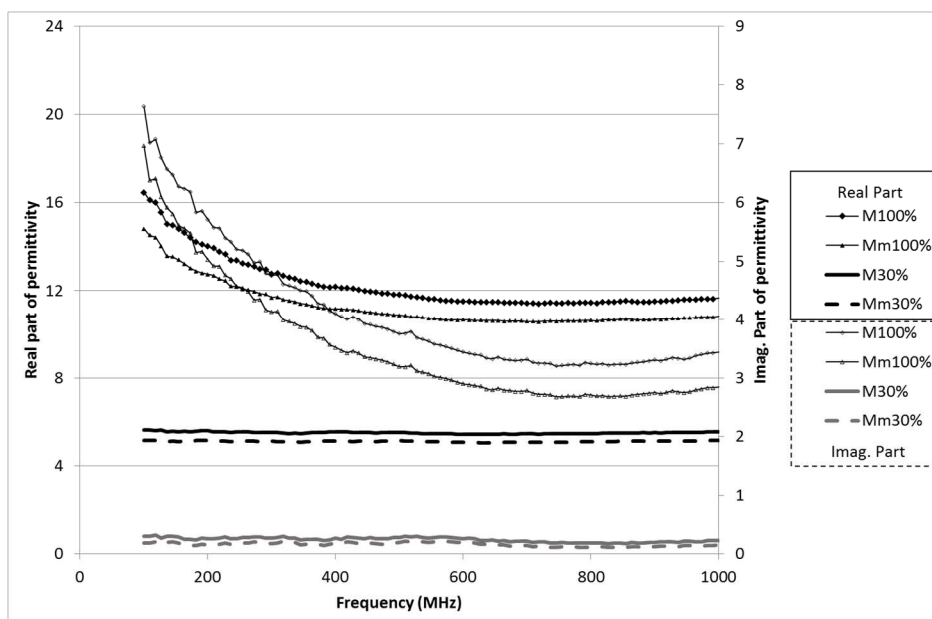


Figure 9: Real and imaginary parts of the permittivity measured on mortars for saturation degrees of 100% and 30%

As for cement pastes, we note that the permittivity is frequency dependent if the saturation degree is high. For the lower saturation degree (30% in this case), neither the real nor the imaginary part of the permittivity depends significantly on the frequency. This dependency observed at high saturation degree is more significant for the imaginary part, as was observed for cement pastes. The effect of moisture is again clearly visible when the values obtained for the fully saturated mortars are compared. Higher permittivity (real and imaginary parts) is measured on mortar M, which has higher porosity. This difference is not significant for the saturation degree of 30% because the volume of water present in the porosity is too small.

In Figure 10, the variation of the real and the imaginary parts of the permittivity are plotted versus the saturation degree for the two mortars. The error bars represent the standard deviation calculated from twelve measurements (one per face of the two available cubes). In comparison with cement paste results, the variation of permittivity is quite continuous here over the whole range of saturation degrees.

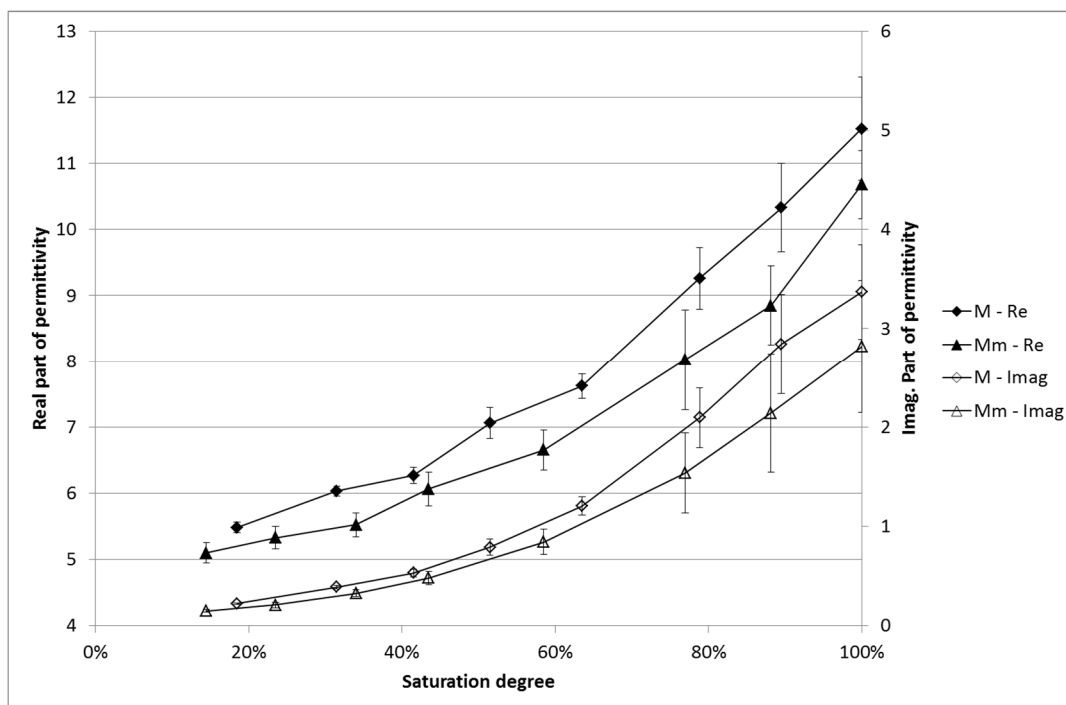


Figure 10: Variation of real and imaginary parts of permittivity (mean in the range 500-1000 MHz) versus saturation degree

5.3. Concrete

The variation of permittivity versus frequency at two saturation degrees (100% and 36%) is plotted in Figure 11. The dispersive behavior is verified again for fully saturated concrete while it seems to vanish for the lower moisture content. This is particularly the case for the real permittivity, whereas the imaginary part of permittivity appears to remain dependent on frequency even for low degrees of saturation. Once again, this variation of permittivity versus frequency is very significant below 500 MHz. For this reason, in the following, as for cement paste and mortar, we will consider the mean of the values measured with the limited frequency range [500-1000 MHz].

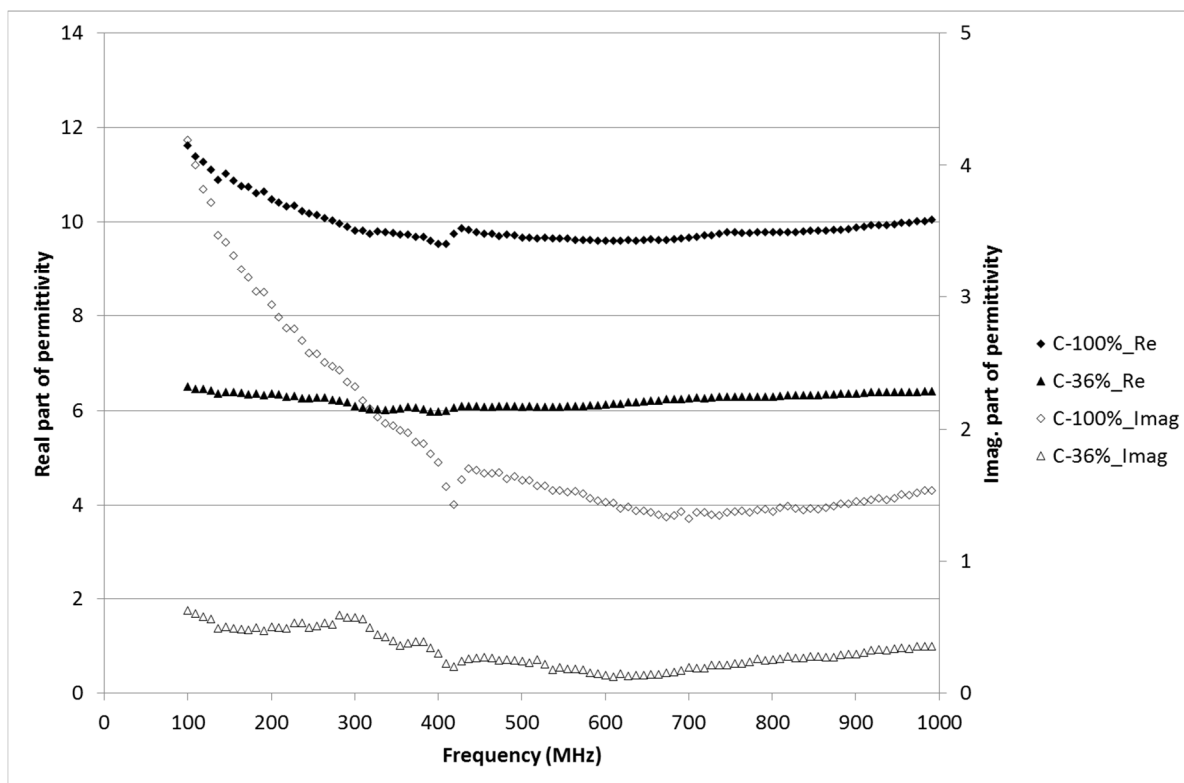


Figure 11: Real and imaginary parts of the permittivity measured on concrete for saturation degrees of 100% and 30%

The variation of permittivity according to saturation degree is plotted in Figure 12. The error bars represent the standard deviation calculated from 18 measurements (one per face of the 9 available slices). The variation could be fitted by a linear relationship between 36% and 90%. But, as for cement pastes, the values measured for fully saturated samples cannot be predicted by this relationship. Due to the fairly low porosity of concrete, the variation remains between 6 and 10 for the real part of the permittivity and between 0.1 and 1.5 for the imaginary part.

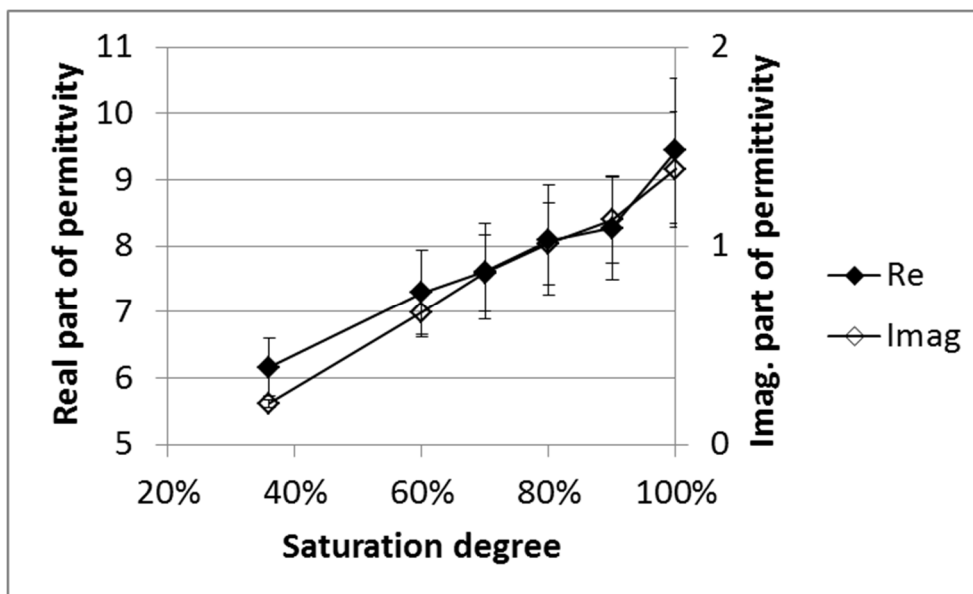


Figure 12: Variation of real and imaginary part of permittivity (mean in the range 500-1000 MHz) versus saturation degree of the concrete

5.3.4. Frequency dependence of permittivity

The variation of real and imaginary permittivity between 100 and 1000 MHz normalized to the mean (normalized variation) is plotted versus the saturation degree for all the mixes in Figure 13. It can be considered that the higher the relative variation is, the higher is the frequency dependence of the mix. It is clear on the figure that the frequency dependence of real permittivity increases (almost linearly) with the saturation degree whatever the mix. The maximum variation of real permittivity is about 40%. Regarding the imaginary part, it can be concluded that there is an increasing trend between the relative variation and the saturation degree, with a maximum significantly higher than for the real part (about 140% obtained for mortar and concrete at 100% saturation). The relative variation is higher for concrete than for mortar or for cement paste. So, a higher frequency dependence of the imaginary permittivity can be expected if the heterogeneity of the mix increases. This effect could be attributed to the presence of the aggregates, which could increase the losses due to interfacial effects. Moreover, the frequency dependence of the real permittivity vanishes for all mixes at the lower saturation degree, as already noted. This can also be observed for the imaginary part of cement paste and mortar but not for concrete, for which results are not available for saturation degree less than 35%. Measurements at lower moisture content should be performed to check whether the frequency dependence vanishes as for mortars and cement pastes.

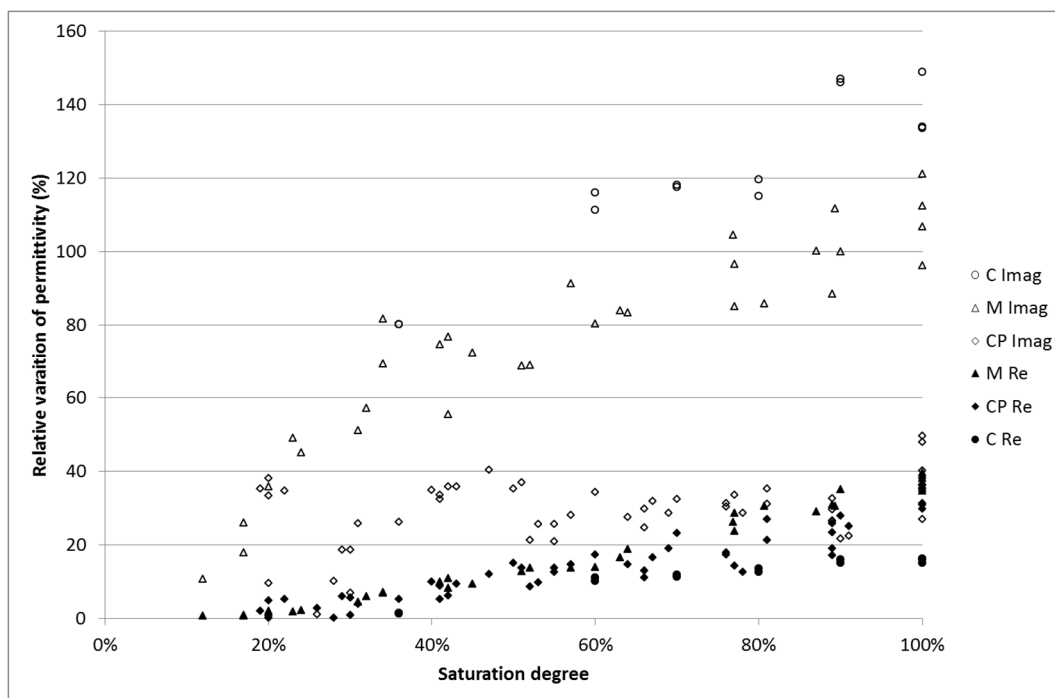


Figure 13: Relative variation of real and imaginary permittivity versus saturation degree

5.4. Relation between permittivity and moisture content

Works can be found in the literature demonstrating that, in cementitious materials or soils, the best correlation between permittivity and moisture is obtained when volume water content is considered instead of the saturation degree [30], [37], [38]. The works involving cementitious materials generally focus on concrete, so the range of porosity is limited to 12 to 20%. In the present work, by involving mortars and cement pastes, we extend the range of porosity up to about 35%. Figures 14 and 15 present the variation of real and imaginary parts of permittivity versus volume water content for all the mixes. In Figure 14, the 6 points corresponding to fully saturated cement pastes are seen to be outside the tendency. If these points are discarded, a single relationship can be drawn between the real part and volume water content for all the mixes, with an acceptable coefficient of determination. It is noteworthy that this relation is determined for quite a large range of moisture content, which is not usual in the literature, where the range is limited to the concrete porosity.

Regarding the imaginary part (Figure 15) different tendencies can be observed. For mortar and concrete, a single tendency can be proposed but a specific relationship is required for cement paste. In this case, the relations are not linear and the best correlation is obtained with an exponential function. Two tendencies can be observed: one for mortar and concrete and the other for cement pastes. In the range [13%-35%] of water content, the imaginary part is higher for mortar than for

cement paste. So it can be concluded that the presence of the aggregates increases the dielectric losses for a given water content – possibly due to interfacial phenomena.

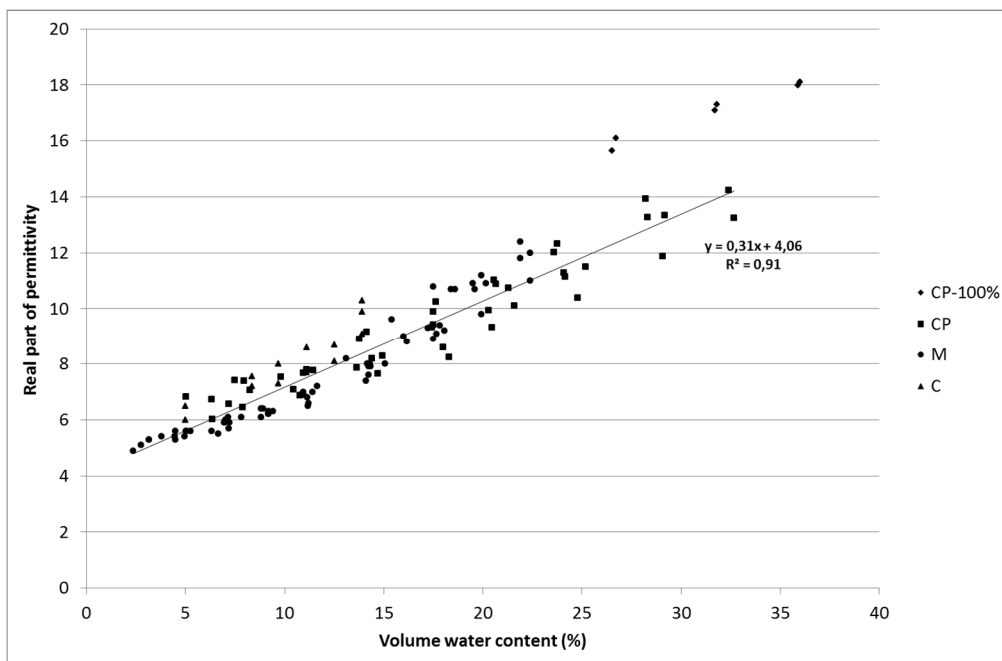


Figure 14: Real part of permittivity versus volume water content for all the mixes

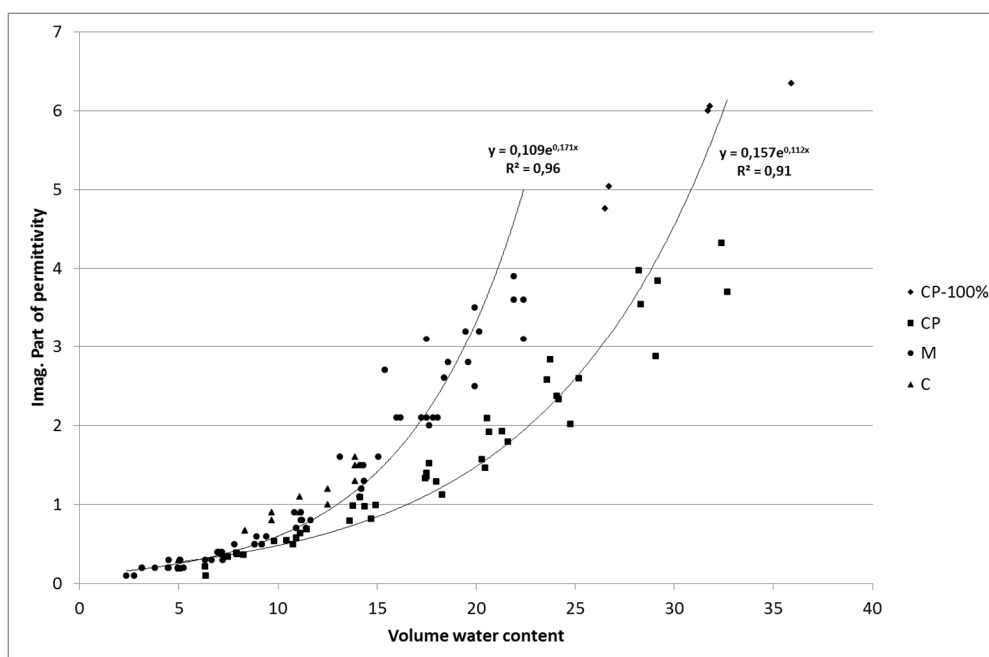


Figure 15: Real part of permittivity versus volume water content for all the mixes

6. Conclusions

This study has focused on an open-ended coaxial probe for measuring the permittivity of different cementitious materials. The open-ended coaxial probe was connected to a portable Vector Network

Analyzer (VNA), Anritsu MS46121, operating at frequencies ranging from 1 MHz to 2 GHz. The measurement method has been described, together with the capacitive model used for measurement processing from the single reflection parameter S_{11} . The different cementitious materials used were: cement pastes having three different water to cement ratios in order to significantly change the porosity, mortars with two different volumes of aggregates, and one concrete. All the mixes used the same cement and the same type of aggregates. The same probe geometry was able to characterize the three cementitious materials.

The results confirm the dispersive behavior of cementitious materials, especially for high saturation degrees. For the real part of permittivity, the dispersive behavior was mainly observed for frequencies below 500 MHz, whatever the material. It was demonstrated that the frequency dependence of the real part, estimated by its coefficient of variation throughout the range of frequency, increased linearly with saturation degree whatever the material (cement paste, mortar or concrete). On the other hand, it was observed that the frequency dependence was significantly higher for the imaginary part of permittivity and was not clearly correlated to the saturation degree. Moreover, the dispersive behavior was globally higher for concrete and lower for cement paste, a characteristic that could be linked to the presence of aggregates.

The results show that the variation rate of real and imaginary permittivity versus saturation degree is not the same over the whole range of moisture content, especially for cement pastes. Between 80 and 100% saturation, the permittivity increased more significantly than in the range [30%-80%].

On the other hand, a single linear relationship could be determined between real permittivity and volume water content in a range of 3% to 35%. Regarding the imaginary part of permittivity, two tendencies were determined, one for cement pastes and one for mortars and concrete.

The coaxial probe presented in this study can be considered as a promising way to determine the permittivity of cementitious materials, and also their components [29], in a frequency range [100-1000 MHz] and over a large range of porosity. As the device can be easily implemented on real sites, it could be used for the calibration of GPR measurements, for a better assessment of wave velocity, for instance.

Future perspectives will concern the development of probes directly embedded in concrete structures to avoid the effects of an air gap between the sample and the probe. Such a probe could be used for monitoring moisture inside concrete structures.

7. Acknowledgements

This work has been performed during the PhD thesis of Vincent GUIHARD funded by Electricité de France (EDF). The French National Agency for Research (ANR “Building and Sustainable Cities”) is also acknowledged for its financial support during the project CONTINUS. Our thanks are extended to Susan Becker, a native English speaker, commissioned to proofread the final English version of this paper.

8. Bibliography

- [1] Dérobert et al., Use of capacitive and GPR techniques for the non-destructive evaluation of cover concrete, *NDT & E International*, Volume 41, Issue 1, January 2008, Pages 44-52
- [2] Chen et al., *Microwave Electronics Measurement and Materials Characterization*, Chapter 3, Reflection Methods, Johan Wiley and Sons, Inc., 2004.
- [3] Stuchly and Stuchly, Coaxial line reflection methods for measuring dielectric properties of biological substances at radio and microwave frequencies - a review, *Transactions on Instrumentation and Measurement*, (3), 1980.
- [4] Popovic D. et al., Precision open-ended coaxial probes for in vivo and ex vivo dielectric spectroscopy of biological tissues at microwave frequencies, *IEEE Transactions on Microwave Theory and Techniques*, 53, (5), 2005.
- [5] Zajicek R. et al., Evaluation of a reflection method on an open-ended coaxial line and its use in dielectric measurements, *Acta Polytechnica*, 46, (5), 2006.
- [6] Boughriet A. et al., The measurement of dielectric properties of liquids at microwave frequencies using open-ended coaxial probes, 1st World Congress on Industrial Process Tomography, Buxton, Greater Manchester, 1999.
- [7] Wagner N. et al., Robust low cost open-ended coaxial probe for dielectric spectroscopy in laboratory and in-situ applications, *Proceedings CMM Conference 2011*, 2011.
- [8] Sheen N. I. et al., An open-ended coaxial probe for broad-band permittivity measurement of agricultural products, *Journal of Agricultural Engineering Research*, 74, 1999.
- [9] You K. Y. et al., A small and slim coaxial probe for single rice grain moisture sensing, *Sensors*, Vol. 13, 2013.
- [10] Skierucha W. et al., A FDR sensor for measuring complex soil dielectric permittivity in the 10-500 MHz frequency range, *Sensors*, 10, 2010.

- [11] Wagner N. et al., Numerical 3d fem and experimental analysis of the open-ended coaxial line technique for microwave dielectric spectroscopy on soil, *IEEE Transactions on Geoscience and Remote Sensing*, 52, (2), 2013.
- [12] Demontoux F. et al., Efficiency of end effect probes for in-situ permittivity measurements in the 0.5-6GHz frequency range and their application for organic soil horizons study, *Sensors and Actuators A: Physical*, (254), 2017.
- [13] Filali B. et al., Design and calibration of a large open-ended coaxial probe for the measurement of the dielectric properties of concrete, *IEEE Transactions on Microwave Theory and Techniques*, 56, (10), 2008.
- [14] Van Damme S. et al., Nondestructive determination of the steel fiber content in concrete slabs with an open-ended coaxial probe, *IEEE Transactions on Geoscience and Remote Sensing*, 42, (11), 2004.
- [15] Komarov A. et al., Open-ended coaxial probe technique for dielectric spectroscopy of artificially grown sea ice, *IEEE Transactions on Geoscience and Remote Sensing*, 54, (8), 2016.
- [16] Moukanda Mbango F., Contribution à la caractérisation électrique de matériaux utilisés en microélectronique radiofréquence, PhD thesis, 2008.
- [17] Jusoh et al., Critical study of open-ended coaxial sensor by Finite Element Method (FEM), *International Journal of Applied Science and Engineering*, 11, (4), 2013.
- [18] Gajda G. B. et al., Numerical analysis of open-ended coaxial lines, *IEEE Transactions on Microwave Theory and Techniques*, 31, (5), 1983.
- [19] McArthur P., Numerical Analysis of Open Ended Coaxial Line Probes and its Application to in vitro Dielectric Measurements, PhD thesis, 1989.
- [20] FEM Analysis of Conical Type Coaxial Open-ended Probe for Dielectric Measurement, *Progress In Electromagnetics Research Symposium Proceedings*, Guangzhou, China, 2014.
- [21] Adous M., Caractérisation électromagnétique des matériaux traités de génie civil dans la bande de fréquence 50 MHz 13GHz. PhD thesis, 2006.
- [22] Ferhat E. et al, Broadband dielectric spectroscopy open-ended probe for the characterization of dispersive materials, *International Conference on Electromagnetic Wave Interaction with Water and Moist Substances*, ISEMA2016, Firenze, Italy, May 23 - 27, 2016.

- [23] Filali B. et al, Measuring dielectric properties of concrete by a wide coaxial probe with an open end, Canadian Journal of Physics Vol. 84, 2006
- [24] Van Damme S. et al., Nondestructive determination of the steel fiber content in concrete slabs with an open-ended coaxial probe. IEEE Transactions On Geoscience and Remote Sensing, Vol. 42, 2511–2521, 2009.
- [25] Misra D. K. et al. A quasi-static analysis of open-ended coaxial lines, IEEE Transactions on Microwave Theory and Techniques, MTT-35, (10), 1987.
- [26] Brady et al. Dielectric behavior of selected animal tissues in vitro at frequencies from 2 to 4 GHz, IEEE Transactions on Biomedical Engineering, 28, (3), 1981.
- [27] Ghannouchi and Bosisio. Measurement of microwave permittivity using six-port reflector with an open-ended coaxial line. Transactions on Instrumentation and Measurement, (38), 1989.
- [28] Elata D. Leus V. Fringing effect in electrostatic actuators. Technical report, Israel Institute of Technology, Faculty of Mechanical Engineering, 2004.
- [29] Guihard V., Taillade F., Balayssac J.P., Steck B., Sanahuja J., and Deby F., Modelling the behaviour of an open-ended coaxial probe to assess the permittivity of heterogeneous dielectrics solids, PIERS Conference St Petersburg, Russia, 22-25 May 2017, Proceedings for IEEE Xplore (Progress In Electromagnetism Research Symposium)
- [30] Dérobert X. et al., EM characterization of hydraulic concretes in the GPR frequency-band using a quadratic experimental design, Non-Destructive Testing in Civil Engineering Nantes, France, 2009.
- [31] GranDuBé. Grandeurs associées à la Durabilité des Bétons, edited by G. ARLIGUIE and H. HORNAIN, AFGC-RGCU, Presses de l'ENPC, Paris, 437 p., April 2007
- [32] Meaney P. M. et al. Open-ended coaxial dielectric probe effective penetration depth determination, IEEE Transactions on Microwave Theory and Techniques, 64, (3), 2016.
- [33] Baker-Jarvis J. et al., Analysis of an open-ended coaxial probe with lift-off for nondestructive testing, IEEE Transactions on Instrumentation and Measurement, 43, (5), 1994.
- [34] Meaney P. M. et al., Microwave open-ended coaxial dielectric probe: Interpretation of the sensing volume re-visited, BMC Medical Physics, 14, (3), 2014.
- [35] Soutsos M. N, Bungey J. H, Millard S. G, Shaw M. R., Patterson A., Dielectric properties of concrete and their influence on radar testing, NDT & E International, Volume 34, Issue 6, September 2001, Pages 419-425

[36] Haddad R. H, Al-Qadi I. L, Characterization of portland cement concrete using electromagnetic waves over the microwave frequencies, Cement and Concrete Research, Volume 28, Issue 10, October 1998, Pages 1379-1391

[37] Klysz G., Balayssac J.P., Determination of volumetric water content of concrete using ground-penetrating radar, Cement and Concrete Research, Volume 37, Issue 8, August 2007, Pages 1164-1171

[38] Topp G. C., Davis, J.L., Annan A.P., Electromagnetic Determination of Soil Water Content: Measurements in Coaxial Transmission Lines, Water Resources Research, Volume 16, N°3, Pages 574-582, June 1980